

ORIGINAL ARTICLE

Pore Size Effect on Mechanical Response and Fluid Permeability for Bone Scaffold Regeneration

Nur Aqila Kadir Hussein¹, Noor Aziah Jamilah Mohtar¹, Luqman Haqim Neza¹, Muhammad Azfar Noordin¹, Amir Putra Md Saad^{1,2}

¹ Applied Mechanics and Design, School of Mechanical Engineering, Faculty of Engineering, Universiti Teknologi Malaysia, Skudai 81310, Johor, Malaysia

² Medical Devices and Technology Centre (MEDiTEC), Institute of Human Centred and Engineering (iHumEn), Universiti Teknologi Malaysia, 81310 UTM Johor Bahru, Malaysia

ABSTRACT

Introduction: The architecture design of bone scaffold plays a vital role in ensuring tissue bone regeneration. Two types of unit and bulk cells with the same geometry are developed with high porosity (86%) to mimic the cancellous bone structure. **Methods:** The mechanical behaviour of bone scaffolds is determined by finite element analysis (FEA), such as elastic modulus and compressive strength. In contrast, computational fluid dynamics (CFD) evaluated the porous magnesium's permeability and wall shear stress. **Results:** The young's modulus of bulk cells of Type A is 2.84 GPa, and Type B is 2.54 GPa tailored to the cancellous bone's mechanical properties (young's modulus: 0.01 GPa – 2 GPa). CFD analysis of permeability result shows a good agreement to mimic the actual bone with the error of 2.20%. **Conclusion:** Therefore, a bigger scaffold geometry exhibited higher permeability and lower wall shear stress in the same porosity.

Keywords: Porous Bone Scaffold, Mechanical Behavior, Permeability, Biodegradable Material, Cancellous Bone

Corresponding Author:

Amir Putra bin Md Saad, PhD

Email: amirputra@utm.my

Tel: +6013-7452154

INTRODUCTION

Scaffold architecture plays a vital role during the bone regeneration process. According to Md Saad & Syahrom (1), the damage of bone tissue in the human body are because of several diseases such as osteoporosis, injury, and trauma. In order to stimulate and guide the bone regeneration process, design variables of scaffolds are currently receiving a lot of attention (1–5). Three-dimensional (3D) pore architecture is a crucial section where the design parameters influence the mechanical properties and mass transportation for nutrient proliferation in order to promote bone ingrowth (6–11). Studies claimed that the effective optimal bone scaffold's porosity is relative from 25-90%, and the best range for pore sizes is from 10-1000 μ m to stimulate bone ingrowth (12-16).

The mechanical properties of scaffolds are fundamental to simulate the compression test when designing the architecture of bone geometry. Respectively, the young's modulus of an ideal scaffold equivalent to the cancellous bone is in a range of 0.01-2 GPa (1). A scaffold should have appropriate mechanical properties consistent with the actual bone, depending on the material used to support bone regeneration (17–21). Mechanically, physiological activities are the ones that cause bone tissue regeneration. This is because external loading triggers bone cells to respond to mechanical stimulation of fluid flow through cancellous bone (6). Various designs of pore architecture could also affect the bone scaffold's mechanical properties and transport behavior (24). According to Syahrom *et al.* (23), the permeability range for cancellous bone is 5.13×10^{-9} - 6.87×10^{-12} m². Therefore, the aim of the work is to study the effect of pore size on mechanical response and fluid permeability by ensuring excellent bone-mimicking to withstand reasonably large deformations at the whole scaffold region.

MATERIALS AND METHODS

This present research study of bone scaffolds understands the usefulness of computational methods using modeling and simulation. In the following section, computational methods used computer-aided design (CAD) and computational fluid dynamics (CFD) software.

Materials

Magnesium is selected because it has adequate mechanical properties suitable to achieve a similar young's modulus relative to the cancellous bone (25). Magnesium has a young's modulus of 3.5 GPa and a poisson ratio of 0.35 (1).

Design of the 3D Models


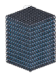


Commercial computer-aided design (CAD) software SolidWorks (Waltham, USA) was used to design the unit and bulk cells from a plate-like structure of sphere-shaped. Table I shows that the plate-like structure consists of two modeling types with different strut and geometry sizes. Hence, Table II illustrated the comparison properties of the unit and bulk model of Type A (0.5mm) and Type B (1.0mm). The surface area and volume for 1mm³ can be obtained from the mass properties table in SolidWorks (Waltham, USA), and the porosity (P) of a unit cell can be calculated by:

$$P = (1 - \frac{V}{V_0}) \cdot 100\% \tag{1}$$

where V_0 is the volume of the solid alloy, and V denotes the volume of the porous structure.

Table I : Type A and Type B models illustrated in a unit cell and bulk model

The composition of the unit cell is from a plate-like structure of sphere-shaped then combine become a bulk structure. The pore size for Type A is 0.5mm, and Type B is 1.0mm.

Type	Pore Size	A unit cell (1x1x1 m ³)	Bulk model (6x6x6 m ³)
A	0.5 mm		
B	1.0 mm		

Mechanical Properties

When designing the architecture of bone geometry, the mechanical characteristics of scaffolds are fundamental for simulating the compression test

using Abaqus (Dassault System Simulia Corp, France). Quantitative terms of mechanical properties such as elastic modulus and yield strength are the most important.

Finite Element Analysis Procedure

In finite element analysis, the model was set young's modulus of 3.5 GPa and a poisson ratio of 0.35. After that, instance assembly was created from a part model and set the state in static, general. Then, two boundary conditions were assigned, one at the bottom surface of the FE model and the other at the top surface of the FE model with a displacement of around 30% of the plastic strain.

Computational Fluid Dynamics (CFD)

Ansys Fluent (ANSYS, Inc., Canonsburg, Pennsylvania) was used to predict the shear stress and pressure drop on scaffold models of Type A and Type B. Before the bulk geometry was imported into Ansys Fluent, modeling is mating with the chamber to analyze a similar condition as in bone marrow. The meshing size is 5.5410⁻⁵ m for the chamber and modeling and 7.5410⁻⁵ m for pipes on both sides of the chamber. This meshing size is selected after conducting a convergence study where a minimum of 1,000,000 elements for an accurate result.

The test rig system provides a laminar flow along the channel length (20.5mm) and varying flow rates (0.25, 0.4, and 0.8 m³/s) in order to represent the human condition during rest, regular and vigorous activities, respectively. The chamber was designed explicitly with a 2-mm inner diameter (D) to clamp and hold the channel of the specimen during testing. Wall shear stress (WSS), pressure drop and permeability values are then evaluated in this analysis. For permeability analysis, Darcy's Law (22) can be expressed as:

$$V_d = \frac{Q}{A_s} = (\frac{kA}{\mu}) \frac{(P_u - P_d)}{L_s} \tag{2}$$

where Q is the volumetric flow rate (m³/s), A_s is the cross-sectional area of the specimen (m²), P_u is the upstream pressure (Pa), P_d is the downstream pressure (Pa), L_s is the specimen length (m), μ is the fluid viscosity, and k is the intrinsic permeability of the specimen (m²).

The viscosity and density of the simulated body fluid (SBF) at body temperature (37 °C) were 1 mPa s and 1000 kg/m³, respectively. The WSS for both models were in laminar flow condition, which in varying flow rates (0.025, 0.4, 0.8 ml/min). A velocity of fluid flow is calculated based on the following:

$$Q = VA \tag{3}$$

where Q is the flow rate of fluid (m^3/s), V denotes the flow velocity (m/s), and A represents the cross-sectional area of pipe (m^2).

Zero pressure at the outlet boundary along a 41-mm exit length was a stationary wall and no-slip condition. The wall shear stress, τ_w from the contour plot can be expressed as (12):

$$\tau_w = \mu \frac{\partial V}{\partial n} \quad (4)$$

where μ is the dynamics viscosity (Pa s), V is the velocity of fluid flow (m/s), and n denotes the x-, y- and z-direction.

Table II : The comparison properties of unit and bulk model of Type A and Type B.

Type of cell	Properties	Unit cell	Bulk cell
A	Volume (mm^3)	0.14	30.50
	Porosity (%)	86	85.88
	Surface area (mm^2)	9.83	2123.45
	Surface area/volume (m^{-1})	70.21	69.62
B	Volume (mm^3)	0.14	31.26
	Porosity (%)	86	85.53
	Surface area (mm^2)	5.01	1081.57
	Surface area/volume (m^{-1})	35.79	34.60

RESULTS

Mechanical Responses

Compressive Stress-Strain Curve Analysis

Fig. 1 illustrated a linear pattern relationship of the stress-strain curve. This is because the properties' input while setting the Abaqus (Dassault Systèmes, Vélizy-Villacoublay, France) only covers the elastic region. As shown below, all of the lines have a positive correlation coefficient ($R^2 = 1$) through a straight-line equation ($y = mx + c$), which shows a perfect positive linear relationship. Fig. 1 analyzed that the unit and bulk cell show a similar trend. Type A (0.5mm) has a stiffer gradient compared to Type B (1mm).

Young's Modulus and Von Mises Stress Criterion Analysis

Fig. 2 shows the magnitude values of young's modulus and von mises stress criterion of each model in order to predict the energy requirements before the geometry fails. Von Mises stress criteria values

show an increasing trend for Type A (0.5mm) unit and bulk cells, which are 1539.55 MPa and 2855.69 MPa, whereas Type B (1mm) unit and bulk cells are 951.82 MPa and 2521.25 MPa. Hence, Fig. 2 presented the values of both cells are exceeding the yield strength of magnesium in the range of 70-140 MPa (26). However, the trend indicates that a smaller geometry size has a higher value of young's modulus and Von Mises Stress Criterion.

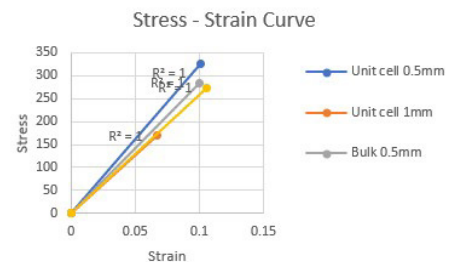


Figure 1 : 100mm x 64mm: Stress-Strain Curve of models, ($R^2 = 1$).

All of the lines have a positive correlation coefficient ($R^2=1$) through a straight-line equation ($y = mx + c$), which shows a perfect positive linear relationship. the unit and bulk cell for Type A (0.5mm) has a stiffer gradient compared to the unit and bulk cell of Type B (1mm) due to the difference in the geometry size of the unit cell

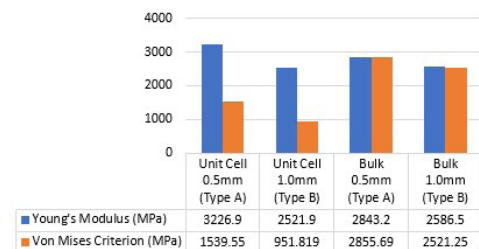


Figure 2 : 116 x 61mm: Magnitude values of Young's Modulus and Von Mises Stress Criterion.

It shows a decreasing trend for unit cells where a unit cell of 0.5mm has a magnitude of 1539.55 MPa while a unit cell of 1mm has a magnitude of 951.82 MPa, which is slightly lower. The trend indicates that a smaller size of geometry has a higher value of young's modulus and von mises stress criterion

Thereby, the smaller the size of geometry, the stiffer the geometry. However, the magnitude of bulk cell Type A and B is slightly similar and still in the range 0.01– 2 GPa of young's modulus of the cancellous bone.

Dynamic Fluid Responses

Pressure Drop

The pressure drop is one of the essential elements, which is computed using Darcy's Law to obtain the permeability value for each specimen type. The pressure drop responses to flow rate under three different flow rates (0.025 - 0.8 ml/min). In all models,

the pressure drops correlated well with flow rates ($R^2 > 0.9997$).

Velocity Distribution

The results are shown in Fig. 3 that displays the entire flow trajectory and velocity distribution for a unit cell’s porous structure. From the contour plots of velocity streamline, the maximum velocity magnitudes are 0.022 till 0.089 m/s for overall Type A (0.5mm) and Type B(1mm) in varying flow rates. Type A with 0.8ml/min flow rate displays the highest maximum velocity. Meanwhile, both Type A and Type B for 0.025 ml/min show the minimum velocity for the most location of elements. As the velocity at the pore circumference increases, the flow rate increases for both types of specimens. As a result, small pore sizes exhibited higher velocity at the pores.

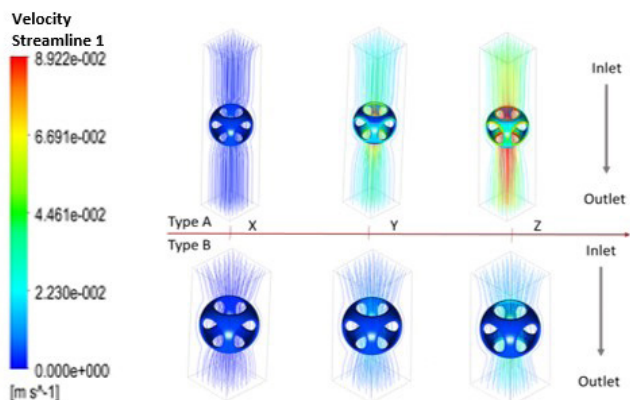


Figure 3 : 125mm x 83mm: Total flow trajectory and velocity distribution unit cell for Type A (0.5mm) and Type B (1mm). The contour plots of velocity streamline, the maximum velocity magnitudes are 0.022 till 0.089 m/s for overall Type A (0.5mm) and Type B(1mm) in varying flow rates. Furthermore, Type A with 0.8ml/min flow rate displays the highest maximum velocity

Wall Shear Stress (WSS)

The distribution of wall shear stress (WSS) in Fig. 4 represented contour plots within various flow rates. Fig. 4 also illustrates the maximum location of shear stress that is marked with a black circle. The flow is considered incompressible flow because the Mach number less than 0.3 ($Ma < 0.3$). Since Type A and B have the same porosity, the WSS increases as the pore is smaller. The maximum shear stress occurs at the area close to the inlet area region as the velocity increase in this region. For instance, this study indicated that a larger pore size would result in more equally distributed WSS. As a result, it might be different from other research due to the viscosity of a fluid, which can affect the wall shear stress and permeability results.

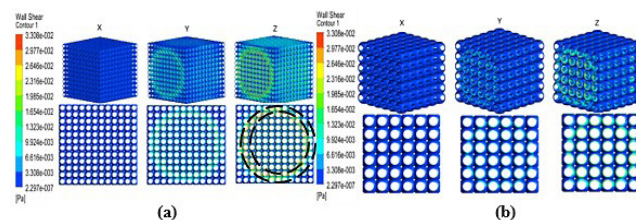


Figure 4 : 156mm x 52mm: The contour plot of shear stress on the porous structure of (a) Type A (0.5mm) (b) Type B (1mm) under various flow rates (Note: X, Y, and Z refers to flow rates of 0.025, 0.4, 0.8 ml/min).

The bulk cell of Type A (0.5mm) exhibits higher average shear stress compared to Type B (1.0mm). The maximum shear stress occurs at the area close to the inlet area region as the velocity increase in this region.

Permeability

Permeability is the ability to transport nutrients throughout the structure. Theoretically, to calculate the permeability can refer to equation (2). The pressure drops from CFD model analysis as a reference to calculate the permeability in each specimen. CFD analysis results show that Type B has higher permeability than Type A, where it is similar to the cancellous bone with an error at 2.20% (23).

DISCUSSION

In this present work, the finite element analysis was performed to simulate the mechanical behavior of the models under load since it is an important criterion to support bone regeneration. Results show that a smaller geometry size is stiffer and requires more energy to force the geometry to deform. The young’s modulus for bulk cells of Type A is 2.84 GPa, and Type B is 2.54 GPa tailored to the cancellous bone’s mechanical properties (young’s modulus: 0.01 GPa – 2 GPa) (1). However, Fig. 2 presented the values of von mises stress criteria for both cells exceeding the yield strength of magnesium in the range of 70-140 MPa (26). This is because the input values for yield strength assumptions are not fulfilled in the finite element analysis, representing the maximum elastic behavior limit. However, the trend shows that small geometry exhibited a higher value of von mises stress criteria. For future studies, a nonlinear analysis should be used as a great solution to identify either linear analysis is acceptable or not and compared with the experiment based.

Furthermore, this study shows that the variation of flow rates used for scaffolds indicates physiological activities of bone marrow movement, affecting the pressure and WSS through the human bone. From the CFD analysis, the maximum average of wall shear stress in a range of 2.34×10^{-7} till 3.34×10^{-2} Pa. However, the shear stress obtained must be in the range of

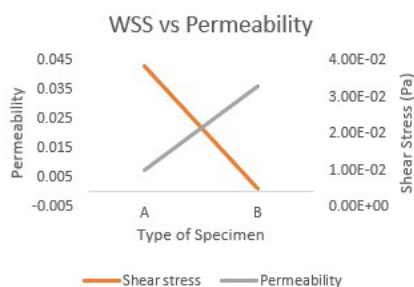


Figure 5 : 90mm x 63mm: Graph of wall shear stress and permeability against the type of specimen.

Both permeability and WSS illustrate the contrast result as it passes through the type of samples. The intersection point is essential to determine the most optimum pore size in the analysis to get the best result from this plate-like scaffold

human cancellous bone, which is 0.1 - 1 Pa (1), in order to generate the optimum shear stress inside the scaffold. When compared to human cancellous bone, the amplitude of WSS in this study is small due to limitations such as using simulated body fluid (SBF) properties as a fluid in the fluid flow test. Thereby, Fig. 5 shows the correlation between wall shear stress and permeability within the specimen. The intersecting point at the intercept line is essential to determine the pore size with the optimum value for permeability and WSS.

In addition, the permeability value obtained from the analysis demonstrated slightly different from the range of permeability based on cancellous bone, which is 5.13×10^{-9} – 6.87×10^{-12} m² (23). This might happen due to the viscosity of SBF that has affected the values of pressure drop obtained from CFD analysis. Current studies show that specimen Type B provides a better permeability value throughout the varying flow rates, resulting in better tissue regeneration. As a result, another study can be conducted to evaluate different geometries utilizing Type A and Type B scaffolds.

CONCLUSION

The porous scaffold has provided better nutrient transport through the human body and eventually speed up the bone remodeling for the fractured bone. This study understands the numerical method to analyze the mechanical properties and fluid permeability depending on the pore size effect, by focusing on magnesium metal. Regarding both geometries of mechanical properties with the same porosity, results show that a bigger structure will have lower young's modulus but higher compressive strength, which indicates more energy required to make the structure deform. Both bulk model types have Young's modulus of 2.84 GPa and 2.58 GPa, respectively, which is relatively close to the cancellous bone Young's modulus range of 0.01-2 GPa (1), which makes it better structure for bone replacement.

Furthermore, CFD results for fluid permeability show a good agreement for both geometry types to mimic the actual bone with an error of 2.20%. However, a bigger pore size provides a better permeability value and lower wall shear stress throughout the varying flow rates, resulting in better tissue regeneration. In this study, plate-like scaffold modeling was found suitable as a replacement for a synthetic bone scaffold. For future studies, the same configuration with other variation designs can be used for experiment-based to compare and validate the result.

ACKNOWLEDGEMENT

This project was sponsored by Ministry of Higher Education Malaysia via the Fundamental Research Grant Scheme (FRGS/1/2018/TK03/UTM/02/8). The authors would like to thank the Research Management Centre in Universiti Teknologi Malaysia (UTM) for managing the project and Center for Information and Communication Technology (CICT) in Universiti Teknologi Malaysia for supporting and providing facilities and services of high-performance computing.

REFERENCES

1. Md Saad AP, Syahrom A. Study of dynamic degradation behaviour of porous magnesium under physiological environment of human cancellous bone. *Corros Sci.* 2018 Feb 1;131:45–56.
2. Zadpoor AA. Bone tissue regeneration: The role of scaffold geometry. *Biomater Sci.* 2015;3(2):231–45.
3. Rahbari A, Montazerian H, Davoodi E, Homayoonfar S. Predicting permeability of regular tissue engineering scaffolds: scaling analysis of pore architecture, scaffold length, and fluid flow rate effects. *Comput Methods Biomech Biomed Engin.* 2017;20(3):231–41.
4. Rakovsky A, Gotman I, Rabkin E, Gutmanas EY. β -TCP-poly lactide composite scaffolds with high strength and enhanced permeability prepared by a modified salt leaching method. *J Mech Behav Biomed Mater [Internet].* 2014;32:89–98. Available from: <http://dx.doi.org/10.1016/j.jmbbm.2013.12.022>
5. Yang X, Lu TJ, Kim T. An analytical model for permeability of isotropic porous media. *Phys Lett Sect A Gen At Solid State Phys [Internet].* 2014;378(30–31):2308–11. Available from: <http://dx.doi.org/10.1016/j.physleta.2014.06.002>
6. Karageorgiou V, Kaplan D. Porosity of 3D biomaterial scaffolds and osteogenesis. *Biomaterials.* 2005;26(27):5474–91.
7. Metz C, Duda GN, Checa S. Towards multi-dynamic mechano-biological optimization of 3D-printed scaffolds to foster bone regeneration.

- Acta Biomater. 2020;
8. Velasco MA, Narv6ez-Tovar CA, Garzyn-Alvarado DA. Design, materials, and mechanobiology of biodegradable scaffolds for bone tissue engineering. *Biomed Res Int*. 2015;
 9. Turnbull G, Clarke J, Picard F, Riches P, Jia L, Han F, et al. 3D bioactive composite scaffolds for bone tissue engineering. *Bioact Mater*. 2018;3(3):278–314.
 10. de Jonge CP, Kolken HMA, Zadpoor AA. Non-auxetic mechanical metamaterials. Vol. 12, *Materials*. 2019.
 11. Mastrogiacomo M, Muraglia A, Komlev V, Peyrin F, Rustichelli F, Crovace A, et al. Tissue engineering of bone: Search for a better scaffold. *Orthod Craniofac Res*. 2005;8(4):277–84.
 12. Zhang L, Song B, Yang L, Shi Y. Tailored mechanical response and mass transport characteristic of selective laser melted porous metallic biomaterials for bone scaffolds. *Acta Biomater*. 2020;
 13. Li J, Zhao Z, Yan R, Yang Y. Mechanical properties of graded scaffolds developed by curve interference coupled with selective laser sintering. *Mater Sci Eng C [Internet]*. 2020;116:111181. Available from: <https://doi.org/10.1016/j.msec.2020.111181>
 14. Basri H, Syahrom A, Saad APM, Rabiatal AA, Akbar Teguh P, Diansyah A, et al. The Effect of Morphology on the Biodegradation Behavior of Porous Magnesium Bone Scaffold. *E3S Web Conf*. 2018;68:1–9.
 15. Giannitelli SM, Accoto D, Trombetta M, Rainer A. Current trends in the design of scaffolds for computer-aided tissue engineering. Vol. 10, *Acta Biomaterialia*. Elsevier BV; 2014. p. 580–94.
 16. Pałka K, Pokrowiecki R. Porous Titanium Implants: A Review. *Adv Eng Mater*. 2018;20(5):1–18.
 17. Kolken HMA, Lietaert K, van der Sloten T, Pourn B, Meynen A, Van Loock G, et al. Mechanical performance of auxetic meta-biomaterials. *J Mech Behav Biomed Mater [Internet]*. 2020;104(January):103658. Available from: <https://doi.org/10.1016/j.jmbbm.2020.103658>
 18. Gao Q, Liao WH, Wang L. An analytical model of cylindrical double-arrowed honeycomb with negative Poisson's ratio. *Int J Mech Sci [Internet]*. 2020;173(December 2019):105400. Available from: <https://doi.org/10.1016/j.ijmecsci.2019.105400>
 19. Noordin MA, Rahim RAA, Roslan ANH, Ali IA, Syahrom A, Saad APM. Controllable Macroscopic Architecture of Subtractive Manufactured Porous Iron for Cancellous Bone Analogue: Computational to Experimental Validation. *J Bionic Eng*. 2020;17(2):357–69.
 20. Torres-Sanchez C, Al Mushref FRA, Norrito M, Yendall K, Liu Y, Conway PP. The effect of pore size and porosity on mechanical properties and biological response of porous titanium scaffolds. *Mater Sci Eng C*. 2017 Aug 1;77:219–28.
 21. Song K, Wang Z, Lan J, Ma S. Porous structure design and mechanical behavior analysis based on TPMS for customized root analogue implant. *J Mech Behav Biomed Mater [Internet]*. 2021;115(November 2020):104222. Available from: <https://doi.org/10.1016/j.jmbbm.2020.104222>
 22. Ali D, Sen S. Finite Element Analysis of Mechanical Behavior, Permeability and Fluid Induced Wall Shear Stress of High Porosity Scaffolds with Gyroid and Lattice-Based Architectures Davar. *J Mech Behav Biomed Mater [Internet]*. 2017; Available from: <http://dx.doi.org/10.1016/j.jmbbm.2017.07.035>
 23. Syahrom A, Abdul Kadir MR, Harun MN, Lichsner A. Permeability study of cancellous bone and its idealised structures. *Med Eng Phys [Internet]*. 2015;37(1):77–86. Available from: <http://dx.doi.org/10.1016/j.medengphy.2014.11.001>
 24. Zadpoor AA, Malda J. Additive Manufacturing of Biomaterials, Tissues, and Organs. Vol. 45, *Annals of Biomedical Engineering*. Springer New York LLC; 2017.
 25. Md Saad AP, Prakoso AT, Sulong MA, Basri H, Wahjuningrum DA, Syahrom A. Impacts of dynamic degradation on the morphological and mechanical characterisation of porous magnesium scaffold. *Biomech Model Mechanobiol [Internet]*. 2019;18(3):797–811. Available from: <https://doi.org/10.1007/s10237-018-01115-z>
 26. Wu S, Liu X, Yeung KWK, Liu C, Yang X. Biomimetic porous scaffolds for bone tissue engineering. *Materials Science and Engineering R: Reports [Internet]*. 2014;80(1):1–36. Available from: <http://dx.doi.org/10.1016/j.mser.2014.04.001>